Plasma Molding over Surface Topography*

Doosik KIM** and Demetre J. ECONOMOU**

A two-dimensional fluid/Monte Carlo simulation model was developed to study plasma "molding" over surface topography. The plasma sheath evolution and potential distribution over the surface were predicted with a self consistent fluid simulation. The trajectories of ions and energetic neutrals were then followed with a Monte Carlo simulation. In this paper, energy and angular distributions of ions and energetic neutrals bombarding an otherwise planar target with a step are reported. As one approaches the step, the ion flux decreases and the ion impact angle increases drastically. For a time invariant sheath (DC case), the ion energy distributions (IED) remain relatively unaffected. When the plasma sheath oscillates at radio frequencies, the IED narrows, while the ion angular distribution becomes broader as one approaches the step. The energetic neutral flux is found to be significant near the vertical step wall. The simulation results are in good agreement with experimental data.

Key Words: plasma molding, sheath evolution, ion energy and angular distributions, Monte Carlo method, plasma etching

1. Introduction

Low gas pressure, high charge density plasmas are used extensively in the processing of electronic materials, especially for etching and deposition of thin films, as well as surface modification.[1,2] Examples of high density plasmas (HDP) include inductively coupled, helicon, and electron cyclotron resonance discharges. The success of plasma processes depends critically on the flux, energy and angular distributions of energetic ions bombarding the substrate. In HDPs, the substrate is usually biased with an independent radio frequency (RF) power supply to accelerate ions towards the surface. Depending on the ratio of the RF time scale ($\sim 1/\omega_{RF}$) to the ion transit time through the sheath, a broad ion energy distribution may result.[3,4] Surface reactions would hardly be affected with low energy ions, while high energy ions may cause damage to the substrate. Also, ions must arrive perpendicular to the surface to ensure etch anisotropy. Therefore, controlling the ion energy distribution (IED) and ion angular distribution (IAD) on the substrate are central goals in plasma processing.[3]

Various analytical or numerical models,[4-8] as well as experimental measurements [9-12] of IEDs and IADs have been reported. In these studies, any surface features on the substrate were extremely small compared to the sheath thickness, i.e., the substrate was effectively planar. There are several applications, however (such as plasma source ion implantation, neutral beam processing, plasma thrusters, and the fabrication of micro-electro-mechanical systems or MEMS), for which the size of features on the substrate can be comparable to or larger than the sheath thickness.[13,14] The plasma would then try to "mold" over the surface topography, i.e., the plasma-sheath boundary or meniscus would not be planar any more. The resulting curved electric field lines can alter the oncoming ion trajectories, greatly influencing the IADs. The ion flux and IEDs along the surface contour can also be affected.

In this article, a two-dimensional (x-y) fluid/Monte Carlo simulation is reported, in an effort to predict the IEDs and IADs on an otherwise planar surface with a step (FIG. 1), in contact with a high density Ar plasma. Energetic (fast) neutrals resulting by neutralization of ions on the wall were also studied. A description of the model and numerical procedures are presented in Sec. 2 and 3. Simulation results are discussed in Sec. 4. Conclusions are drawn in Sec. 5.

2. Fluid Simulation

The compressible fluid equations for ions (species and momentum balances) coupled with Poisson's equation for the electric potential were employed.[2,15] Since the ion temperature is much lower than the electron temperature, the pressure force was ignored in the momentum balance equation. However, ion thermal effects were accounted for in the Monte Carlo simulation. The viscous stress was also neglected in the ion momentum balance. The ion continuity and momentum balance equations would then read

$$\frac{\partial n_i}{\partial t} + \nabla \circ \left(n_i \vec{u}\right) = 0 \qquad (1)$$

* Received on July 31, 2001.

**University of Houston, Plasma Processing Laboratory, Department of Chemical Engineering, Houston, TX 77204-4004, USA

$$\frac{\partial}{\partial t}(n_i\vec{u})+\nabla\circ(n_i\vec{u}\vec{u})=-\frac{en_i}{m_i}\nabla\Phi-\nu_m n_i\vec{u} \qquad (2)$$

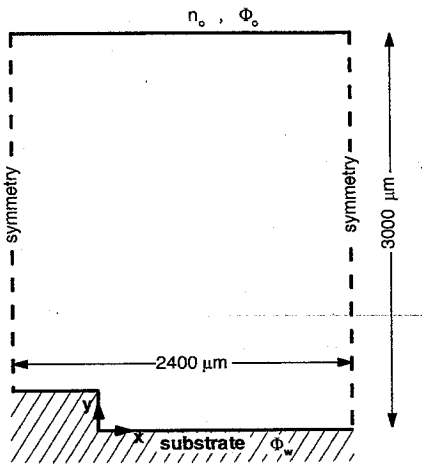

FIG 1: Domain and boundary conditions used for simulations. The substrate step height is 300 μm.

where n_i, m_i, $\vec{u}$, and Φ are the ion density, ion mass, ion fluid velocity vector, and electric potential, respectively. The elementary charge is denoted by e, and ν_m is the ion-neutral collision frequency, where ions could suffer elastic scattering or charge-exchange collisions. Poisson's equation reads,

$$\nabla^2\Phi=-\frac{e}{\varepsilon_o}\left(n_i-n_o\exp\left(\frac{\Phi}{T_e}\right)\right) \qquad (3)$$

where the potential Φ is with respect to that of the upper boundary, Φ_0, ε_0 is the permittivity of free space, and n_0 is the ion density at the upper boundary (FIG. 1). Electrons were assumed to be in Boltzmann equilibrium with the field, and the electron temperature T_e and background gas pressure and temperature (e.g., neutral density) were assumed to be spatially constant. A finite difference scheme was implemented to solve the governing equations. In order to avoid numerical instability and oscillations, the donor cell method was used for all convection terms of the continuity and momentum equations. This method is both transportive and conservative.[16] The equations were integrated in time by an explicit-Euler type method. The time step was chosen so that the Courant-Friederichs-Levy condition was satisfied. At each time step, Poisson's equation was solved iteratively to update the electric potential profile. The simulation evolved until a steady state (for DC cases) or a periodic steady state (for RF cases) was reached.

The system employed in this study is shown in FIG. 1. An otherwise planar substrate with a 300 μm-tall step is located at the bottom of the domain. The potential was specified on the substrate (Φ_w) and at the upper boundary (Φ_o), while both sides were symmetry planes ($\nabla_n\Phi=0$). For RF simulations, both the substrate wall and the upper boundary potentials can be modulated in time. At the upper boundary, the ion density (n_o) was specified but the ion flux (ion velocity) is unknown. When a flux was specified at the upper boundary of FIG. 1, spurious profiles of the ion density near the boundary were observed. The inlet ion fluid velocity (having only a vertical component v_o) was instead linearly extrapolated based on the values at the first two nodes,

$$v_o=2v_1-v_2 \qquad (4)$$

This upstream condition has been used in compressible gas dynamics simulations before.[16] Eq. 4 allows the inlet flux to develop as part of the solution. The specified electron temperature and ion density at the upper boundary set the value of the Debye length at that point. Note that the electron density was set equal to the ion density at the upper boundary, in accordance with the quasi-neutral plasma approximation. The plasma sheath (where charge neutrality breaks down) evolved self-consistently, provided that the upper boundary of the domain was several times thicker than the sheath. The sheath thickness scales with the Debye length. Larger electron densities and lower electron temperatures (smaller Debye length) result in thinner sheath (for given sheath potential).

3. Monte Carlo (MC) Simulation

The MC simulation procedure is summarized in FIG. 2. Ions with the appropriate energy and angular distribution (see below) were launched at a plane near the sheath edge. The location of the sheath edge was defined as the position where the relative net charge is

$$\rho\equiv\frac{n_i-n_e}{n_i}=0.01 \qquad (5)$$

with the densities determined by the fluid simulation. The launch plane was such that the potential distribution was

essentially 1-D on that plane, i.e., the potential at that location was not perturbed by the presence of the step. Ions have a mean energy of the order of the electron temperature at the sheath edge.[17] In addition, ions have energy and angular distributions because of collisions with the background gas in the presheath. The mean directional energy of ions at the launch plane was first evaluated by

$$e_{mean} = \frac{1}{2} m_i \left(u^2 + v^2\right) \tag{6}$$

where u and v are ion fluid velocity components. (the ion fluid velocity at the launch location is essentially perpendicular, i.e., $u \approx 0$.) The perpendicular (directional) energy of entering ions was then determined

$$e_d = e_{mean} \cdot \varepsilon \tag{7}$$

where ε was picked from a Gaussian distribution

$$f(\varepsilon) = A_\varepsilon \exp\left(-\left(\frac{1}{2}\left(\frac{\varepsilon - \mu}{\sigma_\varepsilon}\right)^2\right)\right) \tag{8}$$

with $\mu = 1.0$, $\sigma_\varepsilon = 0.4247$.

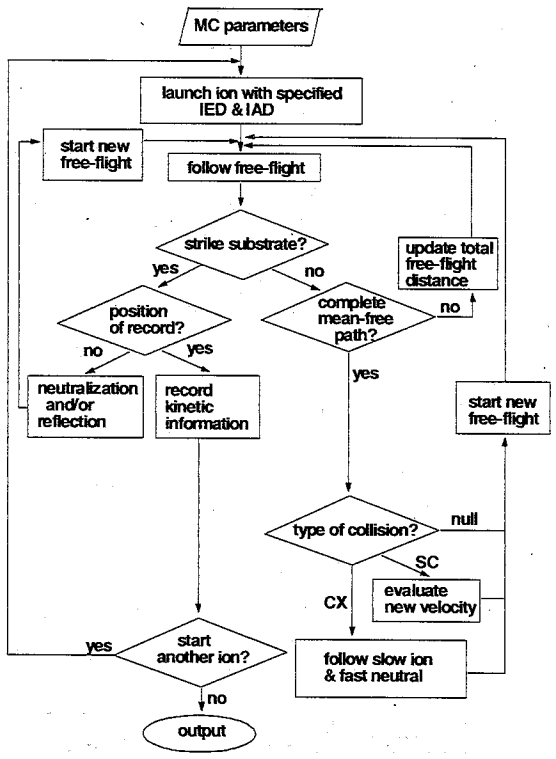

FIG 2: Flow chart for Monte Carlo simulation.

Using Eqs. 7 and 8, one can generate distribution functions similar to those produced by Riemann.[17] For the angular distribution of entering ions, the following formula was used[12]

$$f(\theta) = A_\theta \exp\left(-\left(\frac{1}{2}\left(\frac{\sin\theta}{\sigma_\theta}\right)^2\right)\right) \tag{9}$$

with

$$\sigma_\theta = \sqrt{\frac{T_{i,Tr}}{2e_d}} \tag{10}$$

where $T_{i,Tr}$ is the transverse ion temperature. The angle picked from this distribution was shifted by $\theta_{mean} \equiv \tan^{-1}(-u/v)$ where u and v are again the ion's fluid velocity components at the launching position. Since ions are essentially perpendicular at this point, $\theta_{mean} \approx 0$. This way, the angular distribution of ions at the launch plane was centered at θ_{mean} and had a spread of several degrees.

Once launched ions were accelerated by the spatially non-uniform and time-varying (in the RF case) electric field determined by the fluid simulation. The three spatial coordinates and three velocity components (x, y, z, v_x, v_y, v_z) were tracked in time by a 4th order Runge-Kutta method. During their transit through the sheath, ions can interact with the background neutral gas, *i.e.*, they can suffer elastic scattering or charge-exchange collisions. A constant total cross section σ_t was used to evaluate the distance between collision events by the null collision method.[18] At the end of each free flight, the type of collision was determined according to the probability $P_k = \sigma_k/\sigma_t$ for collision of type k (k can be elastic scattering, charge-exchange, or null collision, i.e., no collision). The cross sections (in units of 10^{-16}cm^2) for elastic scattering (SC) and charge-exchange (CX) collisions between Ar^+ and Ar were obtained from Ref. 2 and fit as follows

$$\sigma_{SC} = 40.04\left(1.0 - 0.0563 \ln \varepsilon_{kinetic}\right)^2 \tag{11}$$

$$\sigma_{CX} = 47.05\left(1.0 - 0.0557 \ln \varepsilon_{kinetic}\right)^2 \tag{12}$$

where the ion kinetic energy $\varepsilon_{kinetic}$ is in eV. Elastic scattering was treated as a hard sphere collision.[19,20] For charge exchange collisions, the (fast) ion and (slow) neutral switched identity (i.e., became fast neutral and slow ion, respectively) without altering their pre-collision velocity vector (resonant process). The resulting energetic (fast) neutrals could suffer elastic scattering further on, which was also treated as hard sphere collision. Fast neutrals, however, were primarily generated by neutralization of ions on the

substrate (wall). Collision with the wall was assumed to result in specular reflection, with 100% neutralization[2] of ions. (More realistic collision models will be implemented later.) Kinetic data for ions and fast neutrals were collected and recorded at four locations on the substrate, to facilitate comparison with experiments: 75, 150, 300, and 1500 μm to the right of the step.

4. Results and Discussion

FIG. 3 depicts the steady-state electric potential profile for an ion density at the upper boundary of $n_o = 10^{17}$ m^{-3}, potential of the upper boundary $\Phi_o = 25$ V, wall potential $\Phi_w = 0$ V (no time modulation, DC case), electron temperature T_e = 2.6 eV, ion temperature T_i = 0.1 eV, transverse ion temperature $T_{i,Tr}$ = 0.1 eV, gas temperature T_g = 0.05 eV, and gas pressure p = 23 mTorr. The electron temperature was measured under these conditions in Ref. 21. The ion temperature was not measured, but was taken as a representative value. [22] The sheath thickness was found to be ~ 350 μm, which is comparable to the step height. As a result, the plasma "feels" the existence of the step and the sheath tries to wrap around the corner. The horizontal electric field (not shown) peaked at the upper corner of the step. Ions are expected to have quite different trajectories depending on their position above the step. The energy and angular distributions of ions recorded at the four locations specified above are shown in FIG. 4. The energy distributions are almost identical in shape and have a width of the order of the electron temperature. This implies that ions gained the same amount of energy (Φ_o-Φ_w) through the nearly collisionless sheath. Due to the horizontal electric field, pulling ions towards the vertical wall (sidewall) of the step, the ion flux (ion count) decreases as the step is approached. The deflection of ion trajectories is also reflected in the angular distribution (FIG. 4b). Higher impact angles (with respect to the vertical) are observed near the step. These ion energy and angular distribution results show good agreement with experimental measurements.[21] Based on these results, one may expect that a considerable portion of the incoming ions are deflected and neutralized at the sidewall of the step. FIG. 5 shows the neutral to ion flux ratio and average impact energy of fast neutrals. A maximum in the flux ratio is seen at a distance of 150 μm from the step; at this location the neutral flux is about 2.5 times larger than the ion flux. The average impact angles of fast neutrals (not shown) were found to be between 30 and 40 degrees. This suggests that the majority of fast neutrals are created by neutralization of deflected ions on the sidewall of the step. Since neutrals produced by charge-exchange collisions were also included, the average impact energy of neutrals is several eV lower than that of ions. It is evident that fast neutrals can have a considerable effect on etching or deposition especially near the step bottom.

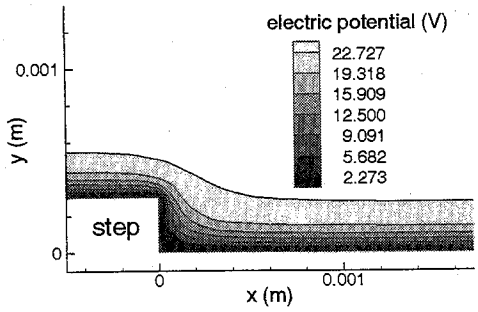

FIG 3: Electric potential profile. $n_o = 10^{17}$ m^{-3}, Φ_o = 25 V, and Φ_w = 0 V.

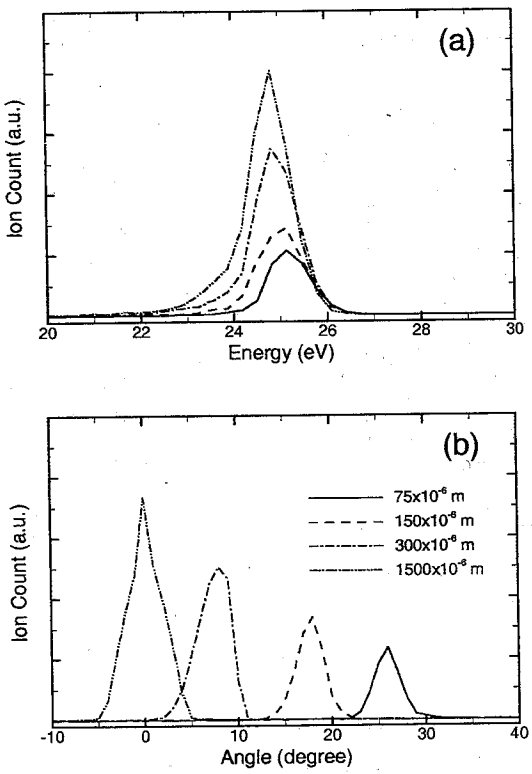

FIG 4: Ion energy (a) and angular (b) distribution at the substrate as a function of axial distance from the step. Same conditions as in FIG 3.

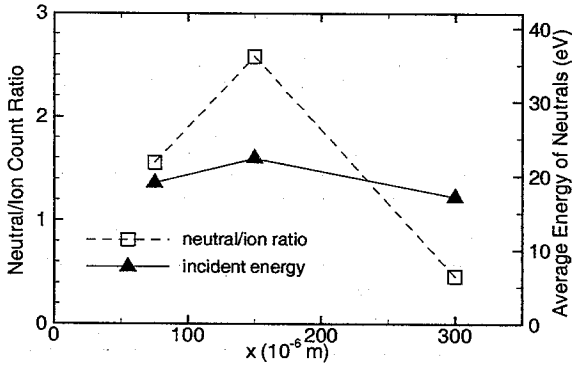

FIG 5: Flux ratio and average impact energy of fast neutrals as a function of axial distance from the step. Same conditions as in FIG 3.

It should be mentioned that the mean free path of ions under the present conditions is a few mm. This is much longer than the sheath thickness (~ 350 μ) but comparable to the computational domain in Fig. 1. Hence ions do not collide in the sheath (where they pick up most of their kinetic energy), but ions suffer on average one collision in their transit towards the sheath.

Results from another steady state (DC) case are displayed in FIG. 6. All conditions were the same as before, except that $n_o = 2\times10^{16}$ m^{-3}. Compared to FIG. 3, a thicker sheath is observed, corresponding to the larger Debye length (lower ion and electron density at the upper boundary). Therefore, the sheath edge becomes less conformal to the solid boundary. The horizontal electric field near the wall is reduced and the nonplanar sheath is extended farther away from the step. As a result, the IAD at a distance of 75 μm is shifted to lower values, while the IAD at 300 μm is shifted to higher values (see FIG. 6b).

The effect of RF sheath modulation can be seen in FIG. 7. Parameter values were $n_o = 3.7\times10^{17}$ m^{-3}, Φ_o = 17+8.5sinω_{RF}t V and Φ_w = -8-10sinω_{RF}t V. The RF modulation frequency was 13.56 MHz. Other conditions were identical to those of FIG. 3. As in the DC cases, energy distributions with essentially the same shape are observed at all locations. Due to the oscillating sheath potential, however, the energy distributions now have a bimodal shape.[4] In addition, the energy spread decreases as one approaches the step. This is due to the fact that the sheath thickness is larger closer to the step. A thicker sheath implies a longer ion transit time and a narrowing of the IED.[4] The ion flux is decreased and the impact angle is increased as one approaches the wall. The sheath modulation is also reflected in the angular distributions. As one is approaching the step, broadening of the distributions is observed. Again, simulation results are in good agreement with experiments.[21]

5. Conclusions

We have developed a two-dimensional fluid/Monte Carlo simulation to predict the energy and angular distributions of ions and fast neutrals impinging on an otherwise planar substrate with a step, in contact with a high density Ar plasma. This is an example of plasma "molding" over surface topography. When the sheath thickness is comparable to or smaller than the step height, ion trajectories near the step are deflected toward the sidewall of the step. The ion flux is reduced and the ion impact angle is increased as one approaches the step. In a DC sheath the ion energy distribution along the lower horizontal surface remains relatively unaffected. Nevertheless, this surface receives a considerable flux of fast neutrals. In the case of RF modulation, the oscillating sheath results in spreading of both the energy and angular distribution of ions. The IED narrows as the step is approached. Simulation results are in good agreement with experimental data.

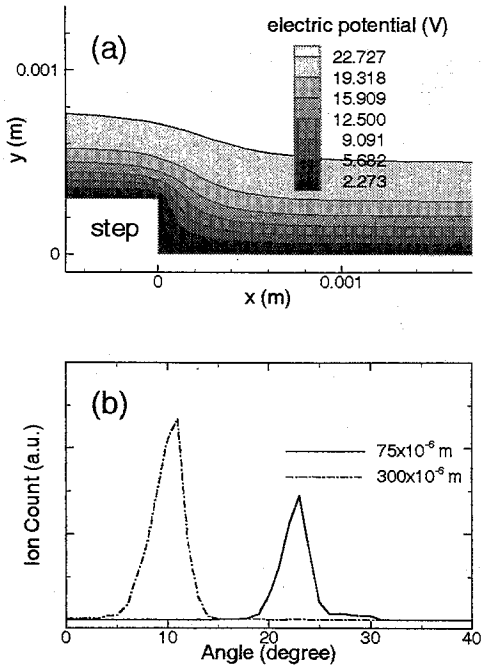

FIG 6: Electric potential profile (a) and ion angular distributions (b). $n_o = 2 \times 10^{16}$ m^{-3}, $\Phi_o = 25$ V, and $\Phi_w = 0$ V.

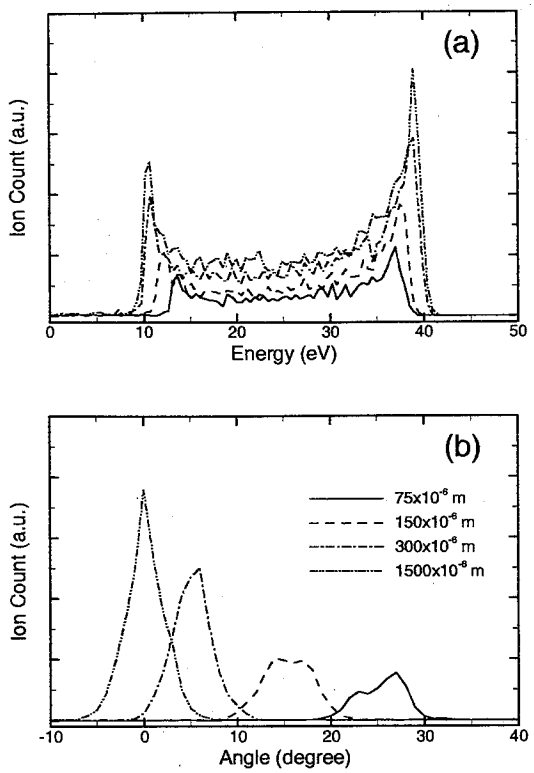

FIG. 7. Ion energy (a) and angular (b) distributions at the substrate as a function of axial distance from the step. n_o = 3.7×10^{17} m^{-3}, Φ_o = 17+8.5sinω_{RF}t V, and Φ_w = -8-10sinω_{RF}t V.

Acknowledgements

Many thanks to Drs. J. R. Woodworth and I. C. Abraham of Sandia National Laboratories for helpful discussions and for sharing their experimental data prior to publication. Financial support was provided by Sandia National Laboratories, NSF (CTS-0072854), and the NSF-supported MRSEC at the University of Houston.

References

(1) S.M. Rossnagel, J.J. Cuomo, and W.D. Westwood (Eds.), Handbook of Plasma Processing Technology, Noyes, Park Ridge, NJ, 1990.

(2) M.A. Lieberman and A.J. Lichtenberg, Principles of Plasma Discharges and Material Processing, Wiley, New York, 1994.

(3) D. J. Economou, *Thin Solid Films*, Vol. 365, (2000), p. 348.

(4) P.A. Miller and M.E. Riley, J. Appl. Phys., Vol. 82 (1997), p. 3689; T. Panagopoulos and D. J. Economou, J. Appl. Phys., Vol. 85 (1999), p. 3435.

(5) E. Kawamura, V. Vahedi, M.A. Lieberman, and C.K. Birdsall, Plasma Sources Sci. Technol., Vol. 8 (1999), p. R45; A. Metze, D.W. Ernie, and H.J. Oskam, J. Appl. Phys., Vol. 65 (1989), p. 993.

(6) M.J. Kushner, J. Appl. Phys., Vol. 58 (1985), p. 4024.

(7) B.E. Thomson, H.H. Sawin, and D.A. Fisher, J. Appl. Phys., Vol. 63 (1988), p. 2241.

(8) M.S. Barnes, J.C. Forster, and J.H. Keller, IEEE Trans. Plasma Sci., Vol. 19 (1991), p. 240.

(9) J. Hopwood, Appl. Phys. Lett., Vol. 62 (1993), p. 940.

(10) M.A. Sobolewski, J.K. Olthoff, and Y. Wang, J. Appl. Phys., Vol. 85 (1999), p. 3966.

(11) E.K. Edelberg, A. Perry, N. Benjamin, and E.S. Aydil, J. Vac. Sci. Technol. A, Vol. 17 (1999), p. 506.

(12) J.R. Woodworth, M.E. Riley, P.A. Miller, G.A. Hebner, and T.W. Hamilton, J. Appl. Phys., Vol. 81 (1997), p. 5950.

(13) I.W. Rangelow and H. Loschner, J. Vac. Sci. Technol. B, Vol. 13 (1995), p. 2394.

(14) U. Czarnetzki, G.A. Hebner, D. Luggenholscher, H.F. Dobele, and M.E. Riley, IEEE Trans. Plasma Sci., Vol. 27 (1999), p. 70.

(15) M. Hong and G.A. Emmert, J. Vac. Sci.Technol. B, Vol. 12 (1994), p. 889.

(16) P.J. Roache, Fundamentals of Computational Fluid Dynamics, Hermosa, Albuquerque, New Mexico, 1998.

(17) K.-U. Riemann, Phys. Fluids, Vol. 24 (1981), p. 2163.

(18) J.P. Boeuf and E. Marode J. Phys. D: Appl. Phys, Vol. 15 (1982), p. 2169.

(19) C.K. Birdsall, IEEE Trans. Plasma Sci., Vol. 19 (1991), p. 65.

(20) J.O. Hirschfelder, C.F. Curtiss, and R.B. Bird, Molecular Theory of Gases and Liquids, Wiley, 1954.

(21) J.R. Woodworth et al. (to be published).

(22) G. A. Hebner, C. B. Fleddermann, and P. A. Miller, J. Vac. Sci. Technol. A, vol. 15 (1997), p. 2698.